Pure Appl. Chem., Vol. 85, No. 11, pp. 2089–2095, 2013.
http://dx.doi.org/10.1351/PAC-CON-13-04-07

Solid-solute phase equilibria in aqueous solution: Fundamentals and applications*,†

Erich Königsberger‡

Chemical and Analytical Sciences, Murdoch University, Murdoch, WA 6150, Australia

Abstract: The importance of solid-solution–aqueous-solution (SSAS) equilibria requires the incorporation of solid solutions into thermodynamic models for industrially and environmentally relevant applications. Insights from appropriate measurements and recent database developments have made such extensions feasible. Examples illustrating various types of stable and metastable equilibria involving solid solutions will be given.

Keywords: aqueous solutions; electrolytes; Lippmann diagrams; phase equilibria; solid solutions; solubility.

INTRODUCTION

Understanding various chemical, geochemical, and physiological processes as well as industrial and environmental problems requires a thorough knowledge of thermodynamic principles and data governing solid-solute phase equilibria in electrolyte solutions. General equations for Gibbs functions of solid and aqueous phases together with parameters determined in simple systems are essential for the prediction of solubilities in complex mixtures over wide ranges of temperature, pressure, and concentration. Upon appropriate differentiation, these equations yield other quantities, including osmotic and activity coefficients, excess enthalpies, entropies, heat capacities, and volumes. These thermodynamic quantities are again related to measurable properties of the substances involved [1].

Solid-solute equilibrium chemistry has often been restricted to pure solids. However, most naturally occurring minerals, as well as solid electrolytes produced industrially, are "solid solutions" (actually, homogeneous solid mixtures), whose solubilities not only depend on those of the respective components (often called "end-members", especially in the geochemical literature) but also on excess Gibbs energies of mixing. Different types of data have been employed for determining excess Gibbs functions of electrolyte solid solutions:

- thermochemical data, i.e., enthalpies of mixing and activities,
- high-temperature phase diagram data,
- low-temperature phase equilibrium data, including
  - miscibility gap data,
  - thermodynamic equilibrium solubilities,
  - stoichiometric saturation solubilities, and
  - distribution coefficient data.

Pure Appl. Chem.* **85, 2027–2144 (2013). A collection of invited papers based on presentations at the 15th International Symposium on Solubility Phenomena and Related Equilibrium Processes (ISSP-15), Xining, China, 22–27 July 2012.
†Dedicated to Prof. Heinz Gamsjäger on his 80th birthday.
‡Corresponding author: E-mail: E.Koenigsberger@murdoch.edu.au

The thermodynamic implications of various types of equilibria between solid and aqueous electrolyte solutions have been developed by Gamsjäger et al. [2–13] and others, e.g., [14–18].

THERMODYNAMICS OF SOLID-SOLUTION–AQUEOUS-SOLUTION (SSAS) EQUILIBRIA

The crucial role of thermodynamics to industrial, geochemical, environmental, and physiological systems involving chemical reactions has been widely recognized. However, the inclusion of solid solutions has traditionally been limited to systems of geochemical importance. Only recently, solid solutions are being implemented in models for hydrometallurgical applications.

The general derivation of equilibrium conditions for binary SSAS systems [3] starts from the total Gibbs energy as a function of the composition of the solid phase, x, and the extent of the dissolution reaction, ξ,

$$dG = (\partial G/\partial x)_\xi \, dx + (\partial G/\partial \xi)_x \, d\xi = 0 \quad (1)$$

This condition can be satisfied in two ways,

$$(\partial G/\partial x)_\xi = 0 \text{ and } (\partial G/\partial \xi)_x = 0 \quad (2)$$

$$dx = 0 \text{ and } (\partial G/\partial \xi)_x = 0 \quad (3)$$

It has been shown [3] that conditions (2) correspond to a stable phase equilibrium characterized by equal chemical potentials of the two components in the solid and aqueous phase, whereas conditions (3) correspond to a constrained, metastable equilibrium involving a solid phase that reacts with constant composition, x. Conditions (3) are equivalent to equal molar Gibbs energies of the two phases [3]; the corresponding constrained equilibria are also known as "stoichiometric saturation" [14]. In the following, these two types of equilibria will be discussed by means of specific examples, together with a third type that is thermodynamically less rigorously defined.

Stable solubility equilibria

The attainment of stable equilibria involves complete recrystallization leading to a homogeneous solid phase with equilibrium composition, which usually requires long equilibration times. This case is frequently found for highly soluble, simple salts such as halogenides [6] or sulfates [18].

Aqueous mixtures of sulfuric acid and metal sulfates are not only relevant for "acid mine drainage" (or other situations where sulfides oxidize in natural environments), but also for acid pressure leaching of latertites or oxidative leaching of sulfide ores. Kobylin et al. have recently developed a Pitzer model for the Fe^{2+}–Ni^{2+}–Mn^{2+}–H^+–SO_4^{2-}–H_2O system [19–21]. Combined with a Pitzer model for the Zn^{2+}–H^+–SO_4^{2-}–H_2O system [22], the solubility of $Ni_{(1-x)}Zn_xSO_4 \cdot 7H_2O$ will be predicted and compared with experimental data [23].

Stable solubility equilibria have been represented graphically in so-called Lippmann diagrams [15], in which "total solubility constants" are plotted vs. mole fractions in the solid and "activity fractions" in the aqueous phase. For a binary solid solution of 1:1 electrolytes MA and NA, $M_{(1-x)}N_xA$, the total solubility product, ΣK_{sp}, and the activity fraction, x_{act}, are defined as

$$\Sigma K_{sp} = (\{M^+\} + \{N^+\})\,\{A^-\} \quad (4)$$

$$x_{act} = \{N^+\}/(\{M^+\} + \{N^+\}) = \{N^+\}\{A^-\}/\Sigma K_{sp} \quad (5)$$

respectively. In eqs. 4 and 5, { } denote activities of ions in the aqueous phase. The equilibrium conditions (2) require that eq. 4 is equal to

$$\Sigma K_{sp} = (1 - x)\gamma_{MA}K_{MA} + x\gamma_{NA}K_{NA} \quad (6)$$

where γ_i and K_i are the activity coefficent in the solid phase and the ("partial") solubility product of component i, respectively. The activity coefficients are related to the molar excess Gibbs energy of the solid phase by eq. 7.

$$G^{E(s)}/RT = (1 - x)\ln\gamma_{MA} + x\ln\gamma_{NA} \quad (7)$$

Equations 5 and 6 define the (lower) "solutus" and (upper) "solidus" curves of the Lippmann diagram, respectively. To relate these quantities to concentrations (i.e., solubilities), activity coefficients of the aqueous species are generally required. Since solubility measurements on sparingly soluble salts are often performed in a background electrolyte medium of constant ionic strength, e.g., [2–4,8,11], activity coefficients are kept constant and activities can be replaced by concentrations. This means that the activity fractions (eq. 5) become mole fractions and the solubility constants are defined in terms of concentrations.

A more convenient representation for highly soluble electrolytes is in terms of $\phi\Sigma m$ (where ϕ is the osmotic coefficient and Σm is the total molality of the two components) and mole fractions in both the solid and the aqueous phase [7]. The product $\phi\Sigma m$ is a thermodynamic potential, which ensures that this solubility diagram is thermodynamically equivalent to a Type II phase diagram, i.e., it is topologically equivalent to the familiar T–x and P–x diagrams [7]. The $\phi\Sigma m$ diagram for $Ni_{(1-x)}Zn_xSO_4{\cdot}7H_2O$ has been calculated with ChemSage [24] and is shown in Fig. 1. ChemSage belongs to the FactSage/ChemApp software family of Gibbs energy minimizers [25]. These programs are capable of calculating phase equilibria and thermodynamic properties for multicomponent systems involving a variety of nonideal phases. For systems of interest to this study, these can be represented by, e.g., the Pitzer model for the aqueous phase and a "subregular" or more complex substitutional model for the solid phase. For a *subregular* mixture, $G^{E(s)}$ is given by

$$G^{E(s)}/RT = x(1 - x)[a_0 + a_1(1 - 2x)] \quad (8)$$

where a_0 and a_1 are dimensionless parameters that can be temperature dependent. For a *regular* mixture ($a_1 = 0$), the thermodynamic conditions for diffusional stability of a phase require that $a_0 < 2$; otherwise, a separation in two phases (demixing) is thermodynamically favored [26]. For alkali halide solid solutions, the excess Gibbs energies, enthalpies, and volumes are generally positive, which has been

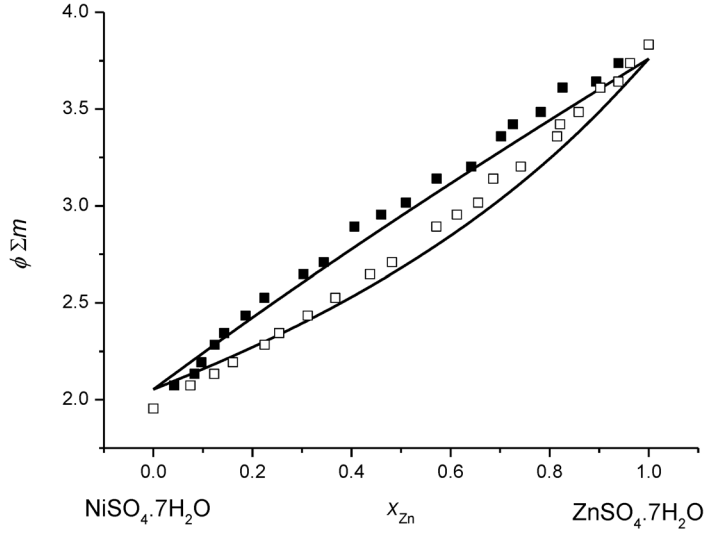

Fig. 1 $\phi\Sigma m$ diagram for $Ni_{(1-x)}Zn_xSO_4{\cdot}7H_2O$ solubilities. Experimental data: solid squares, solid phase; open squares, aqueous phase [23].

correlated with a volume mismatch arising from differences in the end-member lattice parameters [27,28]. In this way, a consistent thermodynamic description of both solid–aqueous and solid–liquid phase diagrams for binary alkali halide systems was achieved [6,28]. Similar correlations between interaction parameters and the volume mismatch of the two end-members have been proposed for other systems [29].

However, for $Ni_{(1-x)}Zn_xSO_4{\cdot}7H_2O$ it has been found that the components mix (almost) ideally in the solid phase [23]. Such close-to-ideal mixing behavior has been attributed to a greater ability of more complex structures to absorb the strain caused by end-member volume mismatch [29]. Given that the experimental solubility and osmotic coefficient data [23] have not been used in the parameterization of the model, the agreement between predicted (assuming ideal mixing, i.e., $a_0 = a_1 = 0$) and measured values is very reasonable.

Constrained, metastable solubility equilibria

Metastable equilibria are attained when the solid solution dissolves congruently, i.e., under the constraint of constant composition of the solid phase. When dissolved in pure solvent (or in a suitable ionic medium), this results in equal mole fractions of solid and aqueous species. Constrained equilibria of this kind are in general found when the kinetics of congruent dissolution is faster than the recrystallization of the original solid solution or the formation of secondary phases (e.g., basic salts). They are common for sparingly soluble salts with similar end-member solubility constants (e.g., transition-metal carbonates). Gamsjäger [2] demonstrated stoichiometric saturation for the dissolution of $Co_{(1-x)}Mn_xCO_3$ solid solutions experimentally and recognized that these metastable equilibria correspond to equal molar Gibbs energy functions of the solid and aqueous phases, which can be represented by an "equal-G curve" (EGC) in Lippmann diagrams [2].

The EGC can be derived from the conditions for metastable equilibrium (eq. 3) and is given by [3,13]

$$\Sigma K_{EGC} = (1 - x) \ln K_{MA} + x \ln K_{NA} + G^{E(s)}/RT \tag{9}$$

Thus, in $\ln \Sigma K_{EGC} - x$ diagrams, the deviation from the straight line connecting $\ln K_{MA}$ and $\ln K_{NA}$ is directly related to the molar excess Gibbs energy of mixing in the solid phase, $G^{E(s)}$.

Flis et al. [30] have recently investigated the solubility of the pyromorphite, $Pb_5(PO_4)_3Cl$–mimetite, $Pb_5(AsO_4)_3Cl$, solid-solution series. This system has gained interest for metals sequestration in water and soil treatment. Flis et al. [30] have found that these solid solutions dissolve congruently and the two components mix ideally in the solid-solution phase. However, their treatment reveals a pitfall that should be avoided in the construction of Lippmann diagrams. The definition of the total solubility constant, ΣK, must be based on one mole of the components that mix in the solid solution (since the Gibbs energy of mixing is an extensive quantity). For the present system, the correct definition of the total solubility constant (solidus line) therefore reads

$$1/3 \log \Sigma K_{sp} = \log\{(1 - x_{As}) [K_{sp}(Pb_5(PO_4)_3Cl)]^{1/3} + x_{As} [K_{sp}(Pb_5(AsO_4)_3Cl)]^{1/3}\} \tag{10}$$

since K_{sp} refers to three PO_4 and AsO_4 groups (Fig. 2, dashed lines). If the exponent of 1/3 in eq. 10 is omitted [30], the resulting Lippmann diagram (Fig. 2, dotted lines) and other derived quantities (e.g., Roozeboom diagrams, Gibbs energies of mixing) are incorrect.

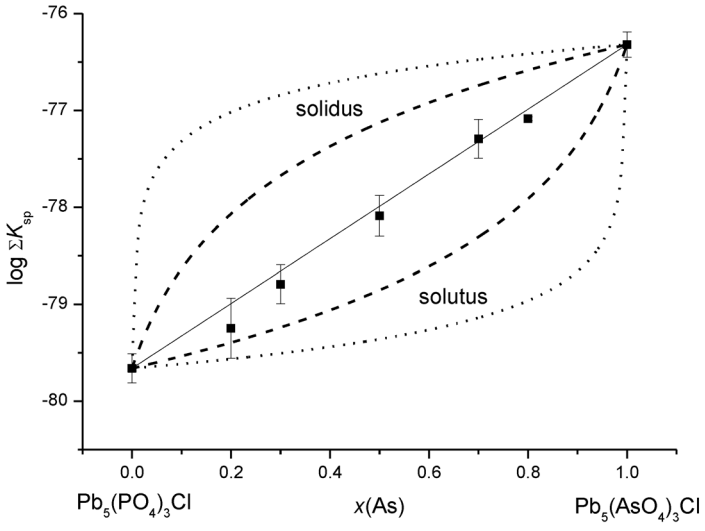

Fig. 2 Lippmann diagram of the pyromorphite, $Pb_5(PO_4)_3Cl$–mimetite, $Pb_5(AsO_4)_3Cl$, solid solution series. Experimental data: squares [30]. EGC, solid; Lippmann diagram with correct (dashed) and incorrect (dotted) Gibbs energy of mixing.

"Primary saturation" and hypothetical end-members

A different type of solubility behavior has been observed for solid solutions with very different end-member solubility constants. In these cases it may appear that the more soluble component dissolves preferentially, leaving the less soluble component behind in the solid phase. However, in many cases, secondary solid phases similar (or equal) to the less soluble component precipitate when the total solubility product exceeds the (lower) "solutus" line of the Lippmann diagram ("primary saturation" [16]). These secondary solid phases may form layers on the surface of the original phase, thus preventing its further dissolution. Prominent examples are magnesian calcites [14] or $Cd_{(1-x)}Ca_xCO_3$ solid solutions [8]. Based on the ionic radii of the components, the latter are regarded as close to ideal, which was experimentally confirmed by direct observation of the (upper) "solidus" line of the Lippmann diagram [8] (in measurements that were similar to precipitation experiments).

In contrast, owing to significantly different radii of Ca^{2+} and Mg^{2+} ions, magnesian calcites should be highly nonideal. This conclusion was also arrived at by solubility measurements under the assumption that magnesite is the second end-member, which suggested a large, positive excess Gibbs function corresponding to an extensive region of demixing. Since magnesite does not precipitate at ambient conditions, it was proposed to describe stable and metastable solubilities of magnesian calcites using a thermodynamically consistent nonideal model of *dilute* solid solutions with a hypothetical, more soluble $MgCO_3$ end-member [10]. This model was capable of explaining results of precipitation experiments leading to ca. 20 mol % Mg-calcites (see ref. [13] for further references and discussion).

A system of industrial importance for the Bayer process is the α-FeOOH (goethite)–α-AlOOH (diaspore) solid-solution series. Calorimetric measurements [31] suggest highly positive excess enthalpies and consequently negligible solid solubility. However, phase-pure Al-goethites with $x(Al) < 0.15$ can be precipitated from aqueous solution at 70 °C [32]. After calculation of mole fractions and total solubility constants from the precipitation data reported in ref. [32], data for the "solidus" line suggest that Al-goethites can be modelled as dilute solid solutions of goethite with a hypothetical "AlOOH" end member (Fig. 3), whose solubility constant is significantly greater than those of diaspore, boehmite, and gibbsite, as calculated from thermodynamic data [33,34]. This dilute solid-solution model is supported by the fact that diaspore does not normally precipitate from aqueous solution under diagenetic

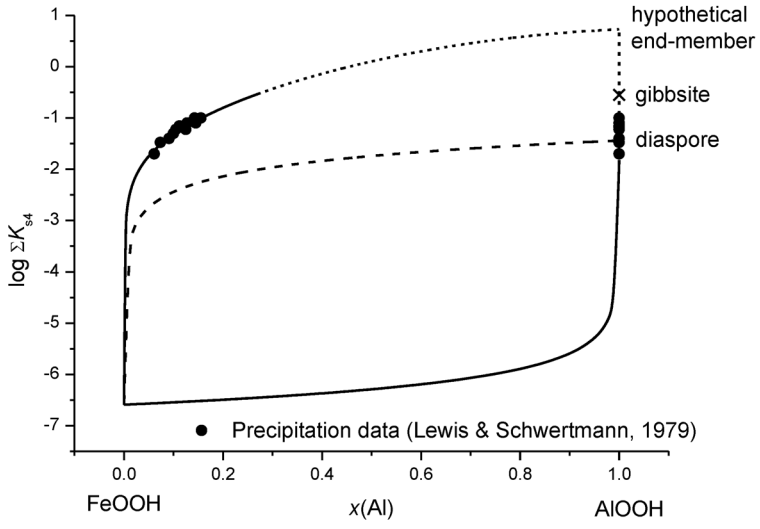

Fig. 3 Lippmann diagram for dilute solid solutions in the α-FeOOH–α-AlOOH system at 70 °C (solid lines). Precipitation data [32] suggest a hypothetical, 'AlOOH' end-member that is more soluble than diaspore, boehmite and gibbsite (×). Solid solutions with $x > 0.27$ are unstable with respect to gibbsite precipitation (dotted lines). Although enthalpies of mixing predict negligible solid solubility in the goethite–diaspore system, the solidus for an ideal mixing model is shown for comparison (dashed line).

conditions [35]. Although a number of experimental observations, particularly regarding the competition between goethite and hematite precipitation [32], can be explained by kinetic rather than thermodynamic considerations, the present model suggests that the maximum Al content in goethite [x(Al) ≈ 0.27]) is limited by the precipitation of gibbsite, in accordance with experimental results [32]. The dilute solid-solution model is not valid outside its parameterization range (dotted lines in Fig. 3).

For the Bayer process, it can be concluded that goethite, if precipitated, may incorporate Al, which results in a loss of product.

The examples discussed in this report indicate that some expert knowledge is required to decide which type of SSAS equilibrium should be considered in the modeling of a particular system.

REFERENCES

1. E. Königsberger, G. Hefter, P. M. May. *Pure Appl. Chem.* **81**, 1537 (2009).
2. H. Gamsjäger. *Ber. Bunsenges. Phys. Chem.* **89**, 1318 (1985).
3. E. Königsberger, H. Gamsjäger. *Ber. Bunsenges. Phys. Chem.* **91**, 785 (1987).
4. E. Königsberger, H. Gamsjäger. *Mar. Chem.* **30**, 317 (1990).
5. E. Königsberger, H. Gamsjäger. *Z. Anorg. Allg. Chem.* **584**, 185 (1990).
6. E. Königsberger. *Monatsh. Chem.* **121**, 999 (1990).
7. E. Königsberger, H. Gamsjäger. *Ber. Bunsenges. Phys. Chem.* **95**, 734 (1991).
8. E. Königsberger, R. Hausner, H. Gamsjäger. *Geochim. Cosmochim. Acta* **55**, 3505 (1991).
9. E. Königsberger, H. Gamsjäger. *Am. J. Sci.* **292**, 199 (1992).
10. E. Königsberger, H. Gamsjäger. *Geochim. Cosmochim. Acta* **56**, 4095 (1992).
11. E. Königsberger, L.-C. Tran-Ho, H. Gamsjäger. *Monatsh. Chem.* **129**, 1061 (1998).
12. H. Gamsjäger, E. Königsberger, W. Preis. *Pure Appl. Chem.* **70**, 1913 (1998).
13. H. Gamsjäger, E. Königsberger, W. Preis. *Aquat. Geochem.* **6**, 119 (2000).
14. D. C. Thorstenson, L. N. Plummer. *Am. J. Sci.* **277**, 1203 (1977).
15. F. Lippmann. *N. Jb. Miner. Abh.* **139**, 1 (1980).

16. P. D. Glynn, E. J. Reardon. *Am. J. Sci.* **290**, 164 (1990).
17. P. D. Glynn, E. J. Reardon, L. N. Plummer, E. Busenberg. *Geochim. Cosmochim. Acta* **54**, 267 (1990).
18. P. D. Glynn. In *Sulfate Minerals*, Ch. N. Alpers, J. L. Jambor, D. K. Nordstrom (Eds.), *Rev. Mineral. Geol.* **40**, Chap. 10, 481–511 (2000).
19. P. M. Kobylin, P. A. Taskinen. *CALPHAD* **38**, 146 (2012).
20. P. M. Kobylin, H. Sippola, P. A. Taskinen. *CALPHAD* **38**, 185 (2012).
21. P. M. Kobylin, H. Sippola, P. A. Taskinen. *CALPHAD* **40**, 41 (2013).
22. E. Königsberger, G. Eriksson. *CALPHAD* **19**, 207 (1995).
23. T. Ojkova, L. Makarow, Chr. Balarew, M. Miloschova. *Z. Phys. Chem. (Leipzig)* **255**, 453 (1974).
24. G. Eriksson, K. Hack. *Metall. Trans. B* **21**, 1013 (1990).
25. G. Eriksson, E. Königsberger. *Pure Appl. Chem*. **80**, 1293 (2008).
26. M. L. McGlashan. *Chemical Thermodynamics*, Academic Press, London (1979).
27. E. Königsberger, H. Schrunner. *Phys. Status Solidi B* **151**, 101 (1989).
28. E. Königsberger. *Z. Phys. Chem. (Leipzig)* **271**, 683 (1990).
29. P. K. Davies, A. Navrotsky. *J. Solid State Chem.* **46**, 1 (1983).
30. J. Flis, M. Manecki, T. Bajda. *Geochim. Cosmochim. Acta* **75**, 1858 (2011).
31. J. Majzlan, A. Navrotsky. *Eur. J. Mineral.* **15**, 495 (2003).
32. D. G. Lewis, U. Schwertmann. *Clays Clay Min.* **27**, 195 (1979).
33. B. S. Hemingway, R. A. Robie, J. A. Kittrick. *Geochim. Cosmochim. Acta* **42**, 1533 (1978).
34. S. Schrödle, E. Königsberger, P. M. May, G. Hefter. *Geochim. Cosmochim. Acta* **74**, 2368 (2010).
35. E. J. Essene, L. M. Anovitz, D. Perkins. *Clays Clay Min.* **42**, 102 (1994).

